PALSAR POLARIMETRY AND INTERFEROMETRY

P122

Hiroshi Kimura [1], *Fumihiko Nishio* [2]

[1] Gifu University
[2] CEReS, Chiba University

1. INTRODUCTION

Polarimetry and interferometry are promising techniques in SAR remote sensing. PALSAR is a advanced SAR after JERS-1 SAR and is expected to have a lot of capabilities for these fields. As for SAR polarimetry, classification and decomposition are important applications. In an urban area analysis by existing methods, it is often found that built-up areas tend to be assigned to strong volume scattering targets. In Section 2, polarization orientation angle shifts are used to discriminate built-up areas. As for SAR interferometry, accurate baseline information is critical for reliable measurements. GPS receives onboard ALOS are expected to derive highly accurate satellite position data (within 1 m) and then enhance interferometric applications. In Section 3, snow cover effects on SAR interferograms are studied. In Section 4, detection of ice sheet and glacier movement inland Antarctica is studied.

2. DISCRIMINATION OF BUILT-UP AREAS USING POLARIZATION ORIENTATION

2.1 BACKGROUND

Polarimetric classification and decomposition are important applications for polarimetric synthetic aperture radar (POLSAR) images. Among many methods developed so far, entropy-anisotropy-alpha classification [1] and three component decomposition [2] are most popular. In an urban area analysis by these methods, it is often found that built-up areas tend to be assigned to strong volume scattering targets. In this paper, polarization orientation angle shifts are used to discriminate built-up areas.

2.2 THEORY

As a polarimetric feature of built-up areas in POLSAR images, the polarization orientation angle shift is known and is given from the scattering model (Fig. 2-1) [3].

$$\tan\theta = \frac{-\tan\alpha}{\cos\phi} \qquad (2\text{-}1)$$

where α is the wall or street orientation angle, and ϕ is the radar incidence angle. From POLSAR data, it is calculated by the circular polarization method [4].

$$\theta = \mathrm{Arg}\left(-\left\langle O_{\mathrm{RR}} O_{\mathrm{LL}}^{*} \right\rangle\right)/4 \qquad (2\text{-}2)$$

where O is the observed backscatter, R and L are the right and the left circular polarization, respectively. It is expected that level ground surface would have always around zero polarization orientation angle independently of the radar illumination direction. If more than two POLSAR images with different look direction (two opposite directions are excluded.) are available, discrimination of built-up areas and the level ground surface would be possible.

2.3 RESULTS

Two ALOS PALSAR images of the Atsugi area, Japan from ascending and descending orbits were used. Firstly, two polarization orientation angle images were generated using (2-2). Next, the two images were ortho-rectified, map-projected and registered. To discriminate built-up areas and the level ground surface, a certain criterion c was applied to the polarization orientation angle from ascending orbit θ_a and that from descending orbit θ_d.

- Built-up area: $|\theta_a|>c$ or $|\theta_d|>c$.
- Level ground surface: $|\theta_a|\leq c$ and $|\theta_d|\leq c$.

Part of the results from ALOS PALSAR polarimetric data of Isehara, Japan is shown in Fig. 2-2. The interest area is dominated by built-up areas and agricultural fields. The polarization orientation angles from the ascending and descending orbits are extremely different (Fig. 2-2 (b) and (c)). Some built-up areas according to the map (Fig. 2-

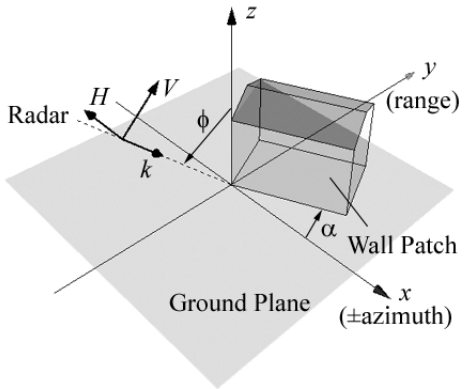

Fig. 2-1 Radar imaging geometry showing the orientation angle of house/building wall

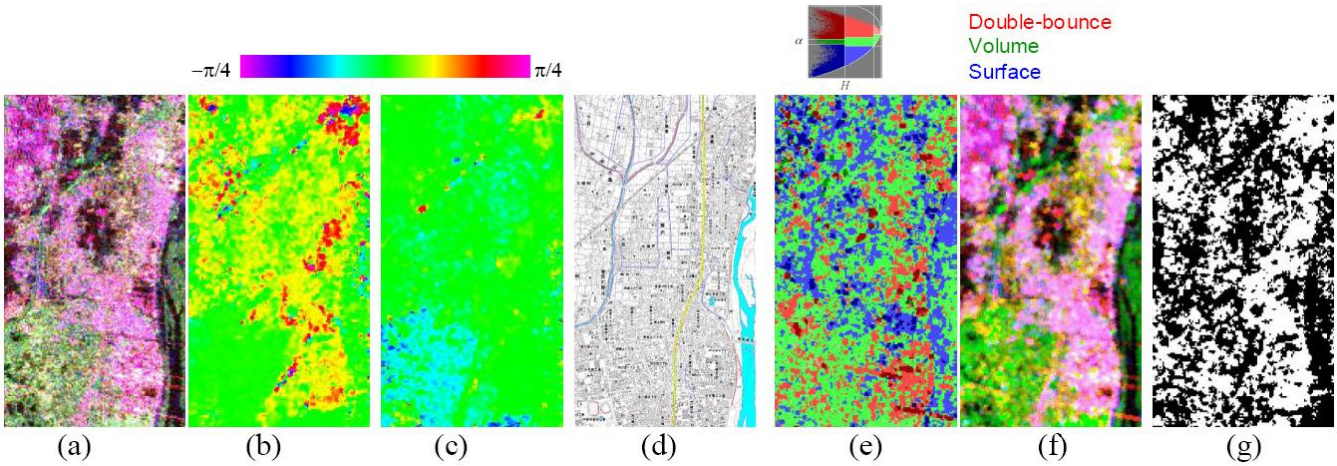

Fig. 2-2 Part of the results from PALSAR data of Isehara, Japan: (a) Pauli vector image from the descending orbit, (b) PO angles from the ascending orbit, (c) PO angles from the descending orbit, (d) Map by The Geospatial Information Authority of Japan (GSI), (e) H-a classification, (f) Three component decomposition, and (g) Built-up areas by the proposed method.

2(d)) are assigned to dipole or vegetation scattering classes (Fig. 2-2(e)) and present a significant amount of volume scattering (Fig. 2-2(f)). The beam azimuth was 100° with the descending orbit and 260° with the ascending orbit. Therefore, c=10° was chosen in the proposed method (Fig. 2-2(g)). The discriminated built-up areas agree well with the map (Fig. 2-2(d)).

3. SNOW DEPTH MEASUREMNT BY SAR INTERFEROMETRY

3.1 BAKGROUND

SAR interferometric technique is used to measure earth surface's topography and movement. The theory is based on that SAR interferograms show differences of radar wave path length between a master and slave images. When the ground is covered with snow, equivalent path length in snow increases. If an image with snow cover is interfered with an image without it, interferometric phases due to snow cover are expected to appear. In this paper, a theoretical relationship between snow cover depth and interferometric phase is derived, and ALOS PALSAR interferograms are analyzed as a case study.

3.2 THEORY

Snow is a dielectric medium and a relative dielectric constant of dry snow is 1.4 to 2.0 [5]. When radar wave passes through snow, it is refracted following Snell's low.

$$\frac{\sin\theta_0}{\sin\theta_1}=\sqrt{\varepsilon_1} \qquad (3\text{-}1)$$

where θ_0 is incidence angle, θ_1 is refraction angle and ε_1 is the relative dielectric constant of snow. In addition, radar wavelength in snow is

$$\lambda_1=\frac{\lambda_0}{\sqrt{\varepsilon_1}} \qquad (3\text{-}2)$$

where λ_0 is radar wavelength in air.

Fig. 3-1(a) shows geometry of radar wave ray. The interfeometric phase brought by snow cover becomes

$$\phi_s=4\pi\left(\frac{l_1}{\lambda_1}-\frac{l_0}{\lambda_0}\right)=\frac{4\pi}{\cos\theta_1}\left[\frac{1}{\lambda_1}-\frac{\cos(\theta_0-\theta_1)}{\lambda_0}\right]d \qquad (3\text{-}3)$$
$$=\frac{4\pi}{\lambda_0}\left(\sqrt{\varepsilon_s-\sin^2\theta_0}-\cos\theta_0\right)d$$

where d is snow cover depth. From (3-3), dry snow cover of 1 meter depth brings 10 to 35 radian interferometric phase at 23 cm wavelength and 30 to 60 degrees incidence as shown in Fig. 3-1(b). Here receiving scattered waves

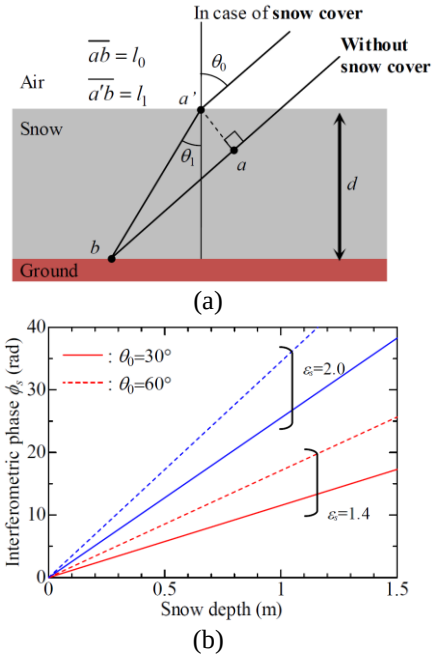

Fig. 3-1 (a)Geometry of wave ray, and (b) Theoretical relationship between snow depth and interferometric phase in case of λ =0.225 m and two kinds of dry snow(ε_1=1.4 and ε_1=2.0).

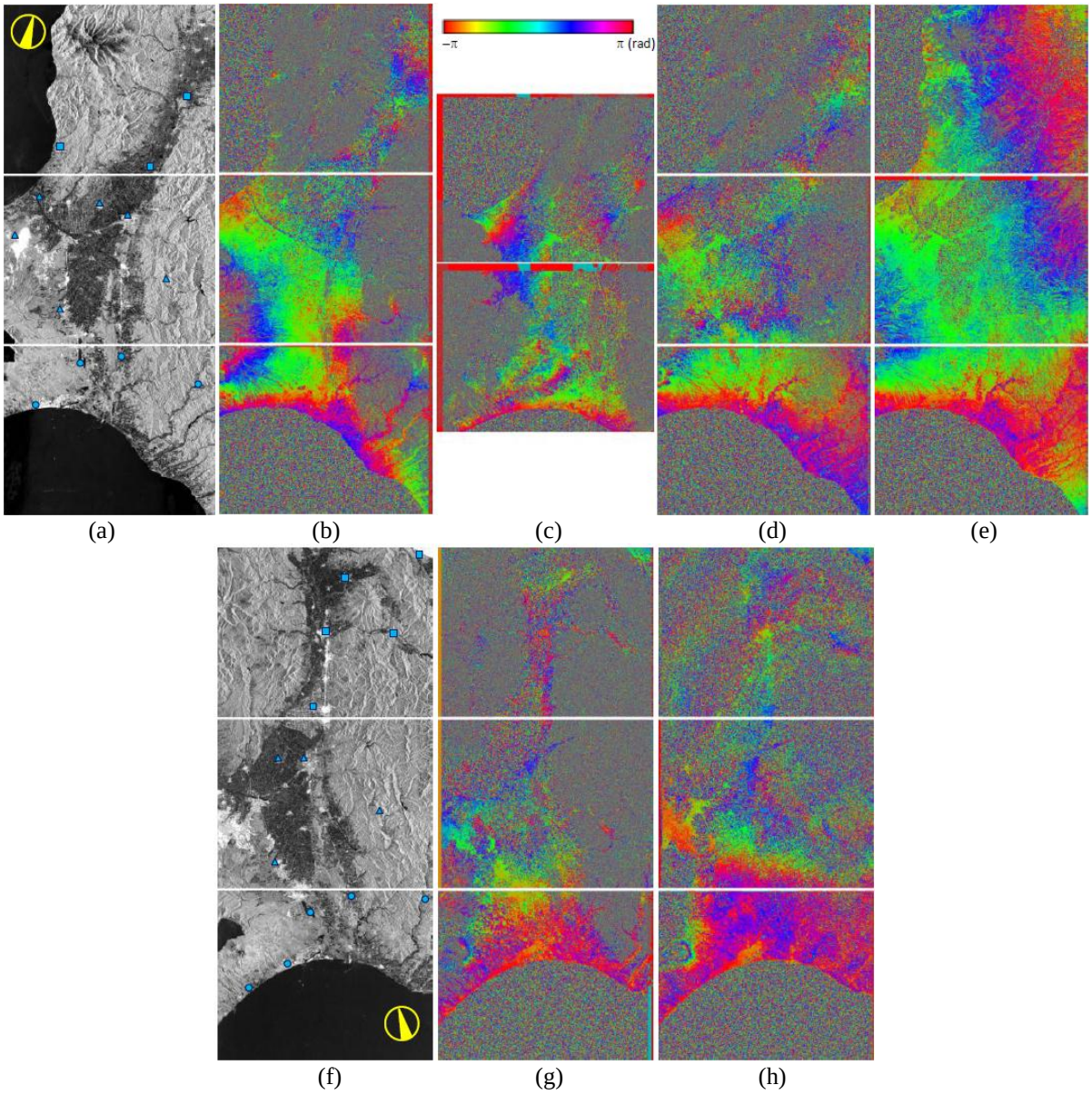

Fig. 3-2 Three consecutive PALSAR amplitude images of the Sapporo region in Hokkaido, Japan. (a)From the ascending orbit, and (f)From the descending orbit. Interferograms after removing flat earth and topographic phases. (b)2007.12.17-2008.05.03, (c)2007.02.20-2006.05.20, (d)2008.02.01-2008.05.03, (e)2008.03.18-2008.05.03, (g)2007.01.11-2007.07.14, and (h)2008.01.14-2007.07.14

3.3 RESULTS

Three consecutive PALSAR scenes over the Sapporo region in Hokkaido, Japan from the ascending and descending orbits were analyzed as shown in Fig. 3-2. Hokkaido is said to have dry snow in winter. During these data acquisition period significant seismic and volcanic activities did not happen. All interferograms were flattened and topographic phases were removed. Interferometric phase was compared with measured snow depth at 13 ground stations of the Meteorological Agency of Japan. It is observed that snow cover degrades interferometric coherency particularly in mountainous areas, but in other areas the coherence is so moderate that phase values can be measured. Phase discontinuity or jump was sometimes detected in urban areas. One of possible reason is snow-removal in relevant areas. Fig. 3-3 is relationships between measured snow depth and PALSAR interferometric phase. Fig. 3-3(c), (e) and (f) show a good correlation between them (R=0.8 to 0.9) and the relative dielectric constant of snow cover is around 1.5. However, others (Fig. 3-3(a), (b) and (d) show a poor

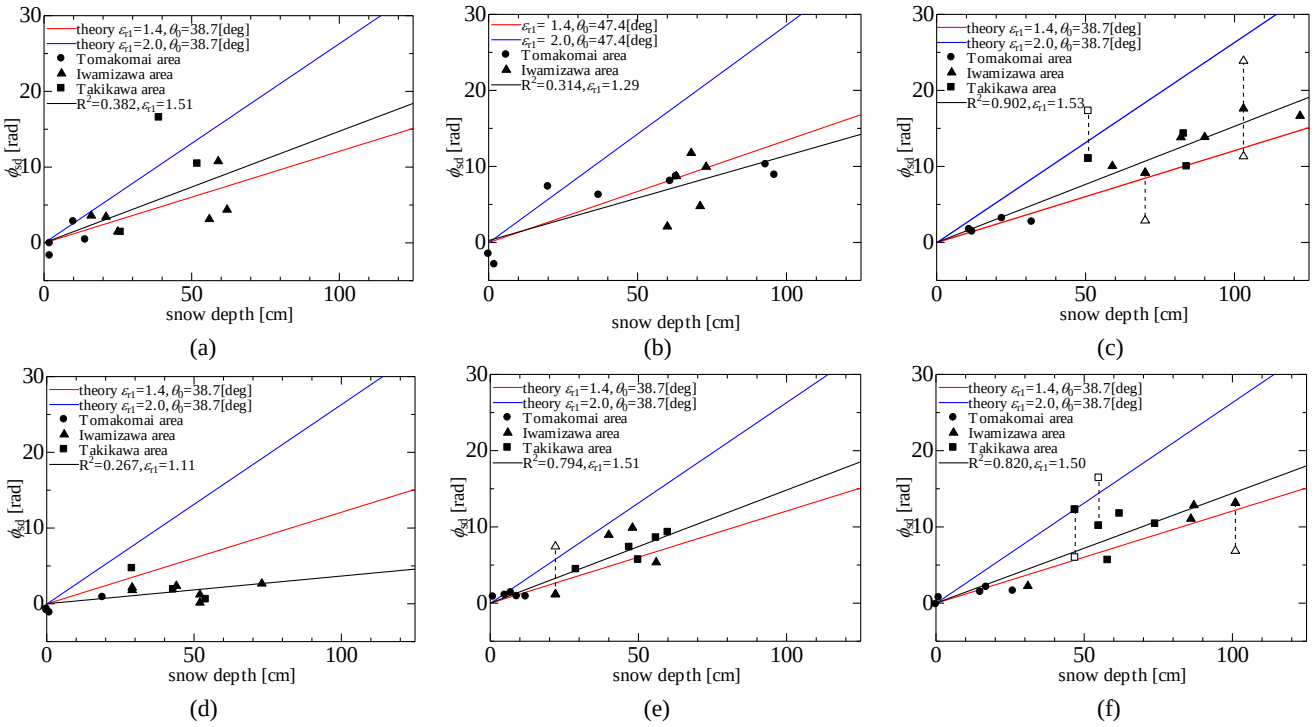

Fig. 3-3 Relationships between measured snow depth and interferometric phase. Shapes of the plots in the figures are corresponding to the locations of ground stations of the Meteorological Agency of Japan shown in Fig. 3-2(a) and (f). (a)2007.12.17-2008.05.03, (b)2007.02.20-2006.05.20, (c) 2008.02.01-2008.05.03, (d)2008.03.18-2008.05.03, (e)2007.01.11-2007.07.14, and (f)2008.01.14-2007.07.14.

correlation. Relation between correlation and perpendicular baseline length is not observed.

4. DETECTION OF ICE SHEET MOVEMENT BY SAR INTERFEROMETRY*

4.1 BACKGROUND

In order to interpret changes in the Antarctic ice as indication of global change on climate, it is necessary to observe the local changes in a regional context. This requires a comprehensive monitoring effort that addresses both the inland ice and changes in the ice margin. Satellite SAR interferometry is expected to provide a promising tool for mapping of glacier and ice sheet movement in the Antarctica. Goldstein et al. [6] and Kwok et al. [7] demonstrated measurements of ice sheet movements using ERS-1 InSAR. With this technology, accurate baselines are critical to precise measurements. As for the late satellite SAR of Japan (i.e. JERS-1 SAR), the orbit information is not good to extract only phases due to surface movement. To overcome this problem and estimate the right baseline, interferometric phases over stable bare rock areas can be used [8]. As for the second generation satellite SAR of Japan (i.e. ALOS PALSAR), accurate baselines from only the orbital information are expected due to GPS receivers onboard ALOS.

4.2 PROCESSING FLOW

Fig. 4-1 shows the processing flow of ALOS/PALSAR data. Errors of the calculated baselines from the orbit data are small, but some fringes sometimes remain in azimuth direction. In the case, remaining phases are flattened so that the phases over stable bare-rock become constant applying the way developed for JERS-1 SAR interferometry for Antarctica. Here GLAS/ICESat 500 m Laser Altimetry Digital Elevation Model of Antarctica was used.

Fig. 4-2(a) and (b) show the PALSAR amplitude mosaic image from 2 by 2 scenes of the Yamato Mountains, Antarctica and the topography of the interest area from the DEM respectively. In Fig. 4-2(a), some bright features are bare-rock areas, and others are rough surfaces. From Fig. 4-2(b), the area has the altitude range of 1600 m to 2600 m, and roughly slops down to the northwest that is nearly parallel to the flight direction.

*: Part of this work was supported by the joint research program of CEReS, Chiba University.

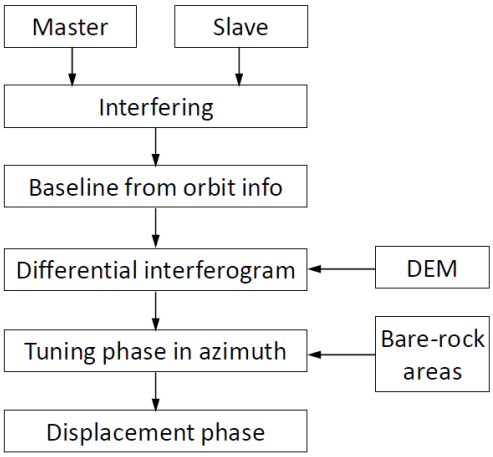

Fig. 4-2 Processing flow

4.3 RESULTS

Fig. 4-3 displays derived interferograms showing ice sheet movement fields. Fig. 4-3(a) and (b) are those of winter and summer respectively. Fig. 4-3(c) and (d) are the InSAR phase differences (summer–winter) from the east path and west path respectively. The difference corresponds to a movement rate change between summer and winter. While the east path (Fig. 4-3(c)) shows a little difference, i.e. -4π in the higher area to $+0.5\pi$ in the lower area, the west path (Fig. 4-3(d)) has a big difference, i.e. -14π in the higher area to $+4\pi$ in the higher area. Particularly the area encircled in white in Fig. 4-3(d) contains a significant difference along the flight direction. Fig. 4-3(e) and (f) are the InSAR phase differences between the adjacent two paths (east–west) in winter and summer respectively. Time difference between two path's interferometric pairs is 12 days for both. The difference of winter (Fig. 4-3(e)) is much smaller than that of summer (Fig. 4-3(f)). This suggests that the big difference shown in Fig. 4-3(d) is not caused by the seasonal variation of the ice sheet movement. The dominant reason of this difference is assumed to be not real motion change but ionospheric effects by aurora activity as shown in [9].

5. CONCLUSIONS

PALSAR data shows new applications for polarimetry and interferometry. The combined use of Polarization orientations from ascending and descending orbits is useful to discriminate built-up areas from others. A possibility of dry snow depth measurement by SAR interferometry is found. Thanks to GPS receives onboard ALOS, accuracy of interferometric measurement would improve. This leads less manual labor in analysis of the Antarctica. As for the Yamato Mountains area, an interferometric analysis does not show large seasonal variations of ice sheet and glacier movement. On the other hand, ionospheric effects by aurora activity are assumed. Such effects should be considered in the future.

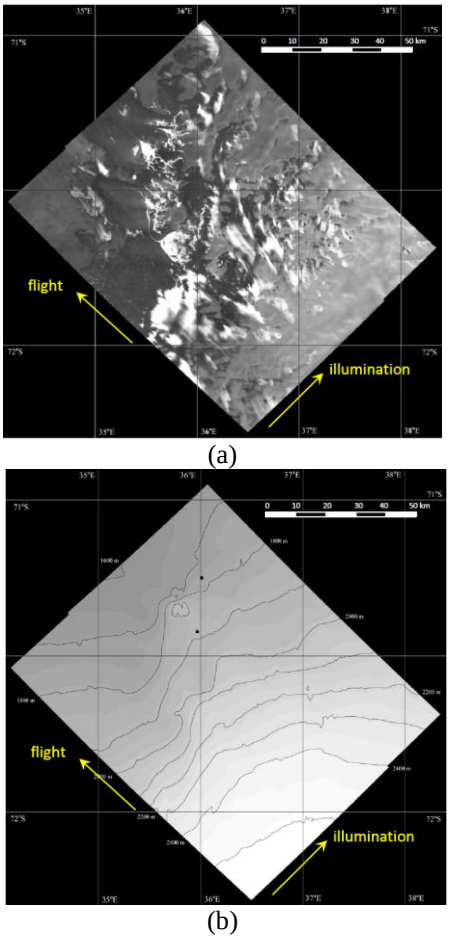

Fig. 4-2 (a) PALSAR amplitude mosaic of the Yamato Mountains, Antarctica, (b) Topography of the interest area from the DEM.

6. ACKNOWLEDGMENT

The authors would like to thank Japan Aerospace Exploration Agency (JAXA) for provision of the PALSAR data for this study. The authors would also like to thank CEReS, Chiba University for provision of some of the PALSAR data described in Section 4.

7. REFERENCES

[1] R. Cloude and E. P. Pottier, "An entropy based classification schene for land applications of polarimetric SAR," IEEE Trans. Geosci. Remote Sensing, vol.35, no.1, pp.68-78, Jan. 1997.

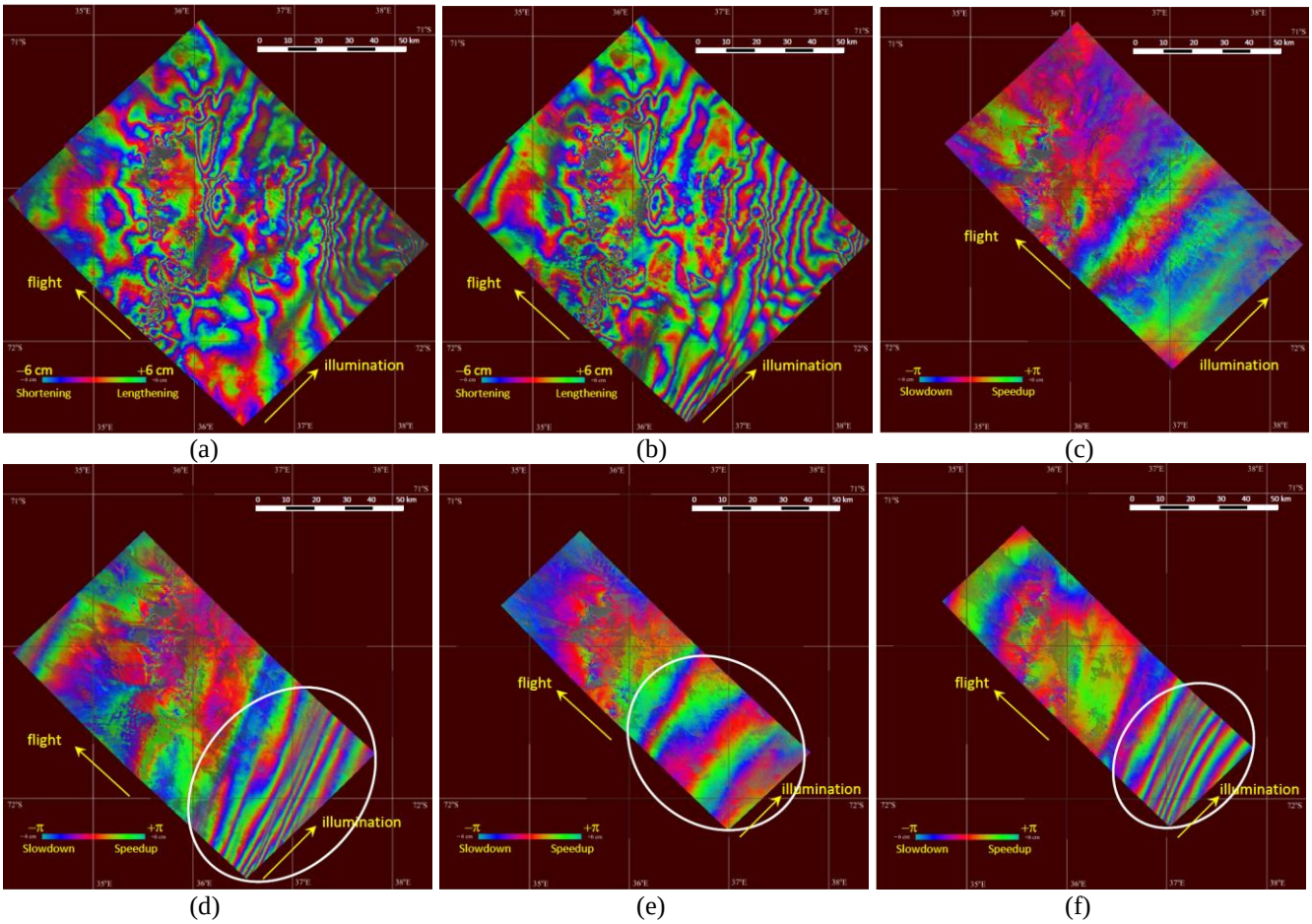

Fig. 4-3 PALSAR interferograms showing the surface movement fields: (a) Winter, (b) Summer. Differences of InSAR phase differences between summer and winter (summer–winter): (c) East path, (d) West path. Differences of InSAR phase between two adjacent paths (east–west): (e) Winter, (f) Summer.

[2] A. Freeman and S.L. Durden, "A Three-Component Scattering Model for Polarimetric SAR Data", IEEE Trans. Geosci. Remote Sensing, vol.36, no.3, pp.963-973, May 1998.

[3] H. Kimura, "Radar polarization orientation shifts in built-up areas," IEEE Geoscience and Remote Sensing Letters, vol. 5, no. 2, pp.217–221, Apr. 2008.

[4] J. S. Lee, D. L. Schuler, and T. L. Ainsworth, E. Krogager, D. Kasilingam and W-M Boerner, "On the estimation of radar polarization orientation shifts induced by terrain slopes," IEEE Trans. Geosci. Remote Sensing, vol. 40, no. 1, pp. 30–41, Jan. 2002.

[5] F.T.Ulaby, R.K.Moore and A. K. Fung: MICROWAVE REMOTE SENSING ACTIVE AND PASSIVE VOLUME II, p.828, ARTECH HOUSE INC., 1982.

[6] Goldstein R. M., H. Englehardt, B. Kamb and R. M. Frolich, "Satellite radar interferometry for monitoring ice sheet motion: Application to an Antarctic Ice Stream," Science, vol. 262, no. 1, pp. 525-1,530, 1993.

[7] R. Kwok and M. A. Fahnestock, "Ice sheet motion and topography from radar interferometry," IEEE TGRS, vol.34, no.1, 189-220, 1996.

[8] H. Kimura, T. Kanamori, H. Wakabayashi and F. Nishio, "Ice Sheet Motion in Inland Antarctica from JERS-1 SAR Interferometry," Proc. of 2004 IEEE International Geoscience and Remote Sensing Symposium, 2004.

[9] F. Meyer, "A review of ionospheric effects in low-frequency SAR – Signals, correction methods, and performance requirements," Proc. of 2010 IEEE International Geoscience and Remote Sensing Symposium, 2010.